Fault-tolerant passively integrating in-vivo dosimeters for feedback-enabled proton therapy (IF^{2}D, or Integrating Feedback F-center Dosimeter)

by

Rossana Iturbide

SUBMITTED TO THE DEPARTMENT OF NUCLEAR SCIENCE AND ENGINEERING IN PARTIAL FULFILLMENT OF THE REQUIREMENTS FOR THE DEGREE OF

BACHELOR OF SCIENCE IN NUCLEAR SCIENCE AND ENGINEERING AT THE MASSACHUSETTS INSTITUTE OF TECHNOLOGY

JUNE 2018

Signature of Author:_____

Rossana Iturbide
Department of Nuclear Science and Engineering
May 18, 2018

Certified by:_____

Michael P. Short
Professor of Nuclear Science and Engineering
Thesis Supervisor

Accepted by:_____

Michael P. Short
Professor of Nuclear Science and Engineering
Chairman, Committee for Undergraduate Students

Fault-tolerant passively integrating in-vivo dosimeters for feedback-enabled proton therapy (IF^2D, or Integrating Feedback F-center Dosimeter)

by

Rossana Iturbide

Submitted to the Department of Nuclear Science and Engineering on May 18, 2018
In partial Fulfillment of the Requirements for the Degree of
Bachelor of Science in Nuclear Science and Engineering

ABSTRACT

Current dosimeters used in radiotherapy for cancer treatment fail to distinguish between radiation received by the targeted tumor and the surrounding healthy tissue. The Integrating Feedback F-center Dosimeter is designed to be fault-tolerant, with the capability to distinguish the radiation dose received between a targeted tumor and surrounding tissue. To provide a proof of concept of the IF^2D, five alkali halide salts will be irradiated by a tandem electrostatic proton accelerator. These salts, (NaCl, NaI, NaBr, NaF, CsF), were chosen for their f-center properties which enable a direct conversion between the wavelength of the irradiated salt i.e. color change, and the expected radiation dose. We expect that analytical calculations between wavelength and expected radiation dose will correlate with experimental data. A direct conversion will enable the doctor to determine how much radiation the salt has received and therefore how much radiation dose the tumor itself has received. As a result, the patient will require less exposure time, and less radiation treatments, thus reducing the probability of obtaining secondary cancers. The following paper outlines the initial procedures taken to irradiate the selected salts and theoretical calculations that we expect to parallel future experimental data.

Thesis Supervisor: Michael P. Short

Title: Professor of Nuclear Science and Engineering

Contents

1 Introduction

1.1 Motivation

Radiotherapy for cancer treatment has lacked real time, fault-tolerant, feedback-controlled dosimeters. This results in oncologists' inability to reliably measure and control radiation dose during therapy treatments. These radiation therapy treatments include radiation from protons, x-rays or implanted brachytherapy. Various factors contribute to the inability to measure radiation dose to a tumor and surrounding tissue in real time including organ movement, and the inability to record correctly the dose received during hardware or software failures.

Over the last fifty years, advancements in dosimeter technology have failed to address the need for a fault-tolerant, real time, feedback controlled dosimeter. Developments in dosimeter technology include implanted, online, and proportional scintillators, which provide limited information in terms of fault-tolerant and accurate target dose. Scintillating dosimeters are limited in that the entire data collection must be intact, so they are vulnerable to faults in equipment and data collection.

1.2 Primary Application

The proposed design of the IF^{2}D consists of a set of implantable salt crystals that change color with ionizing radiation due to the creation of f-centers. Vacancies in the salt can absorb photons at specific wavelengths, and these can be correlated to dose. The IF^{2}D is passively integrating so that the salts change color with ionizing radiation regardless of the data acquisition setup, and as a result the total dose can be read at any time. This solves the problem current dosimeters have, and makes the IF^{2}D fault-tolerant because a failure in the data acquisition setup does not lead to a failure in response of the device itself. The IF^{2}D allows radiation oncologists to receive dose information as it occurs, which in turn allows the device to be implanted once, avoiding invasive implantations and extractions.

1.3 Project Overview

Current dosimeters also fail to determine the precise dose to the tumor and to the surrounding healthy tissue. Often, the prescribed dose to a tumor cannot be achieved in a single treatment because of co-irradiation to healthy tissue and secondary cancers from the radiation treatment. Different organs, tissues and glands absorb radiation differently and move around even if the patient is lying still. As a result, predictions are made prior to the radiation treatment concerning dose received by the tumor and the surrounding tissue, or measured after the radiation treatment. A dosimeter capable of providing real-time measurements would enable doctors and patients to confidently know the correct dose was delivered to the tumor, minimizing dose exposures. This thesis research project will provide a proof of concept for a fault-tolerant, passively integrating in-vivo dosimeter for feedback-enabled radiation therapy. The implantable dosimeter will consist of various

implantable salt crystals, optical fibers, and a handheld spectrometer. By the end of the project, the absorption at specific wavelengths obtained experimentally by irradiating the salts with a tandem electrostatic accelerator will be compared to theoretical data as a proof of concept.

2 Background

2.1 Proton Therapy

The goal of cancer therapies is to remove and/or destroy cancerous tissues in patients, while limiting damage to healthy tissue. Cancer therapy consists of surgery, chemotherapy, radiation, and immunotherapy [1]. Radiation therapy can be administered through an external beam or via radionuclides. Until the 1990s, external beam photon therapy was more commonly used than proton therapy. However, interest in proton therapy rose from the physical properties of protons that provide dose control between the cancer target and surrounding healthy tissue.

Dose control is a particularly difficult problem in cancer therapy. Organ motion in patients from natural tasks like breathing make it hard to penetrate cancerous tissue versus healthy tissue. As a result, covering the cancerous region is often given priority rather than limiting the radiation exposure to healthy tissue. This can become a significant problem due to secondary cancers, caused by the radiation exposure to healthy tissue.

Photon therapy uses megavoltage photons from a gantry-mounted linear accelerator (LINAC) [1]. The gantry allows the photon beam to rotate around the patient and provide treatment at different angles. This rotation is necessary because of photon characteristics. Because photons are uncharged, the radiation dose they deposit is indirect via secondary electrons. As seen in the following figure, the photon dose distribution curve shows a maximum dose at lower depths, and the energy deposited decreases with increasing depth. For non-superficial tumors, multiple photon beam angles are required to guarantee a higher dose to the targeted region.

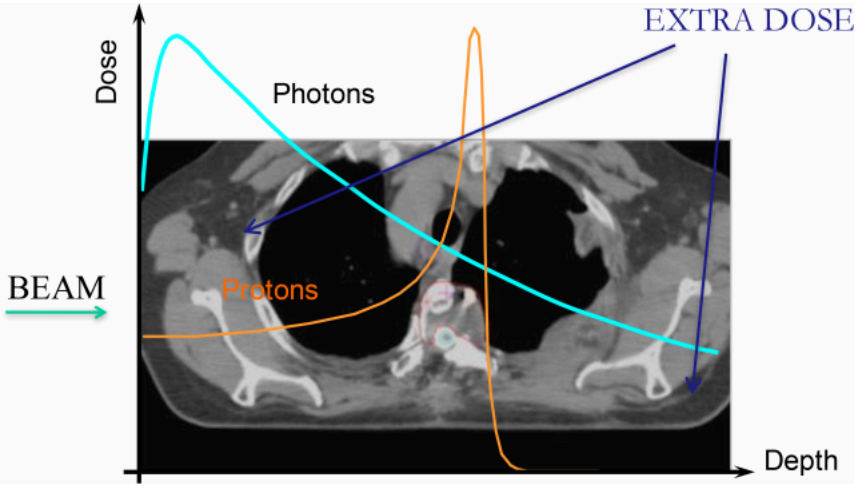

Figure 1 Depth vs. Dose distribution of a photon beam (blue) and proton beam (orange). The photon beam displays a maximum dose at a small depth whereas the proton dose reaches a maximum at a higher depth (where this results in a Bragg curve) *[1]*.

Protons are heavy charged particles unlike photons, that interact with materials. Protons have a finite range in tissue because they interact with electrons and nuclei in the material and lose kinetic energy per unit distance in the material, as denoted by the stopping power of charged particles $\frac{-dT}{dX}$ [2]. Characteristic Bragg peaks for protons allow for a larger deposit of energy at a concentrated depth in the target tumor. Unlike photon therapy, a single dose can provide the radiation dose to the desired location without the need of multiple angles. An important characteristic of proton therapy is that the tail end of the dose vs. depth curve trails off long before the photon therapy curve, which deposits energy to non-targeted tissue. One example of where energy deposition outside of the tumor area matters is in pediatric brain cancer patients. Any additional dose to the surrounding healthy tissue can have adverse effects on: cognitive development and/or bone growth [1].

Some impracticalities in proton therapy involve the accelerators needed to generate the proton beams. These particle accelerators are large and are situated outside of the multiple treatment rooms they feed. The accelerators require magnets that help transport the proton beam to patients by bending, steering and focusing the beam. On the other hand, photon therapy LINACs and their beam shaping/monitoring devices fit into one room. In order to obtain the most efficient orientation, proton therapy also requires gantries. Whereas the photon gantry is used to deliver multiple doses, the proton gantry works to provide the correct orientation. This requires a full 360-degree gantry if other arrangements can't be provided that will rotate the patient himself [1].

2.2 F-Centers

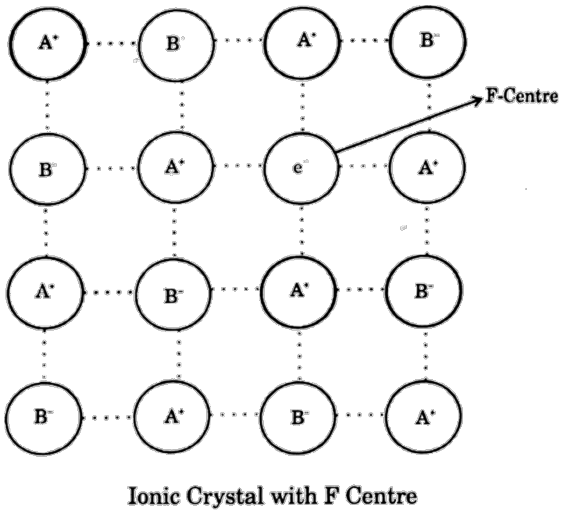

Figure 2 Generalized ionic crystal composed of elements A and B. F-center shows a halide vacancy filled by an electron *[3]*.

Color centers are imperfections and occur in inorganic solids at the atomic scale. These imperfections can be impurities, vacant lattice sites, or interstitial atoms [4]. A common color center if an F-center, which results from the absence of an electron from a point in the solid. That is, when an atom changes its position in the crystal lattice, it forms a halide vacancy [5]. The vacancy acts like a positively charged particle and traps an electron. Trapped electrons or holes due to these imperfections lead to color changes in the solid because their energy changes the absorption spectrum of the material. F-centers in NaCl for example, absorb blue light, and therefore the typically colorless solid obtains a yellow tinge. If the trapped electron leaves the halide vacancy, then the color center also disappears, reverting the salt to its colorless and clear form [6]. The color the salt displays varies with different levels of radiation, which allows for a correlation between radiation dose and absorbed wavelength. For example, if a salt absorbs an increasing amount of radiation, the color change in the salt increases. Using a spectrometer to measure the color change, we can determine how much radiation the salt has received. Color changes can be observed at low radiation energies and would therefore be prevalent in the desired proton therapy range of 70-250 MeV [7].

2.3 Current Dosimeters

An ideal dosimeter for intensity modulated radiation therapy IMRT consists of the following qualities: [8] [9]

- Determines absolute dose
- Provides three-dimensional data
- Response is not orientation-dependent
- Well-calibrated
- Data supports readout

- Absolute dose measurement is insensitive to dose rate and radiation energy
- Non-toxic
- Reasonable cost to build and maintain

Additionally, we want the following qualities added:

- Dose information is returned in real-time
- Used in-vivo
- Easy to implant and remove, and does not impose a health risk to the patient
- Fault tolerant

The following dosimetry techniques have been considered for in-vivo and/or real-time feedback applications: prompt gamma monitoring, PET scans, and MOSFET dosimeters.

2.3.1 Prompt gamma monitoring

The interactions between radiation and tissue can result in emitted secondary radiation. The emitted secondary radiation from a patient can provide the amount of radiation deposited at a specific location. In proton therapy one type of secondary radiation deposited in patients are prompt gammas [10]. In order to obtain the real-time and location-specific dose of a patient, prompt gammas can be correlated to radiation dose [11]. Since prompt gamma detection correlates to the range of protons in a target, detection could theoretically be used to confirm maximum dose to tumor cells and not to healthy tissue.

Prompt gamma monitoring has several disadvantages. First, Gueth et al. suggests that the correlations at specific tissues with specific doses are "mostly unknown under real conditions" [12]. Second, prompt gamma detection is not sufficiently accurate and it is expensive. There is significant noise in detection, and therefore monitoring requires equipment with higher sensitivity which is more expensive in order to provide more accurate readings. Furthermore, prompt gamma detection and monitoring is designed for proton therapy and is not designed for general radiation therapies that use other particles. [9]

2.3.2 PET scans

Positron emission tomography (PET) scans are another dosimetry tool similar to prompt gamma monitoring as radiation excites specific isotopes. Positrons emitted by excited isotopes are of interest in PET scans. Positrons detected at specific locations via their 511keV annihilation gamma rays indicate a correlation between the amount of radiation deposited and that tissue location. PET and prompt gamma detection both aim to enable a real-time dose monitoring that would allow dose corrections in the beam in real-time as well [9].

While Knopf et al. proposed PET as a way to verify the depth of the radiation beam, the method faces difficulties for some targeted areas in the body [13]. Particularly in soft

tissues, the calculated location of gamma-ray emission is not the same with the original proton-tissue interaction because of diffusion [14]. PET scans as a form of dosimetry is also expensive like prompt gamma detection and would require complex methods for measurement in order to obtain a continuous and reliant electronics-software setup through the irradiation procedure [9].

2.3.3 MOSFET dosimeters

During radiation treatments, the ionizing radiation creates electron-hole pairs in the gate oxide of metal-oxide semiconductor field-effect transistors (MOSFETs). Compared to the electrons, the holes have a lower mobility. Electrons recombine quickly which allows some mobility between the gate oxide and silicon substrate. There is a finite probability that the hole will be trapped by interface defects that arise from strain when the hole reaches the interface. The threshold voltage needed to open the channel between the source and the drain contacts changes with increasing positive charge at the oxide-substrate interface because it modifies the formation of a depletion layer when the gate oxide is biased. This means that through calibration there is a direct correlation between the threshold voltage change and the dose received at the gate [15].

Unlike diode-based dosimeters, MOSFET dosimeters do not need to add bias in order to collect radiation dose information. The trapped holes don't have short lives so they don't require a constant applied voltage and measurements can be made at regular intervals after completing a radiation treatment.

Beyer et al. used MOSFET dosimeters in prostate cancer patients and found that measured doses were significantly different from the prescribed radiation dose and sometimes by more than 5% [16]. Preliminary results from a wireless, implantable MOSFET dosimeter is shown in the following figure. The histogram shows the percent difference between the measured radiation dose and the prescribed dose in the 20 patients that participated in the clinical trial for breast cancer treatments.

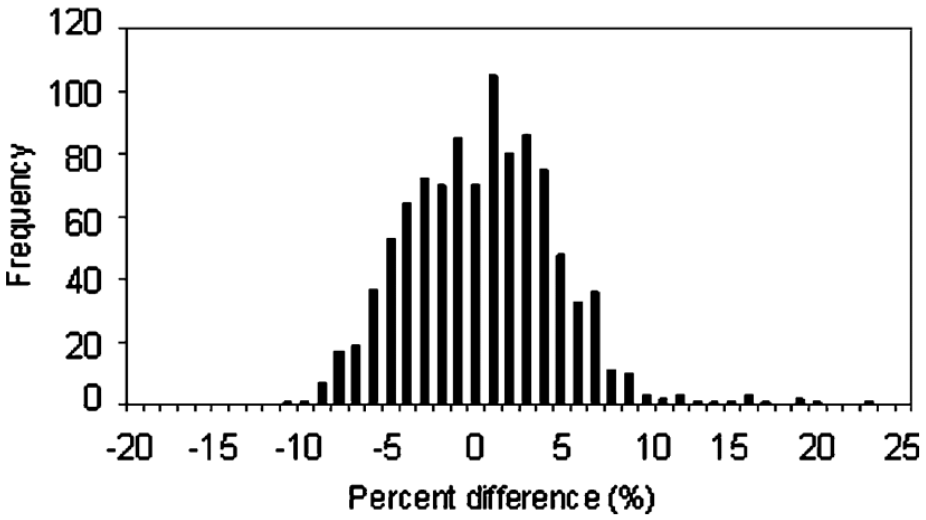

Figure 3 Histogram of the percent difference between the prescribed radiation dose and the measured dose in 20 clinical trial breast cancer radiation treatment patients using in-vivo MOSFET dosimeters [11].

2.4 Proposed IF^{2}D

The proposed IF^{2}D will include the following qualities that have not yet been developed in other dosimeter technologies:

- Dose information is returned in real-time
- Fault-tolerant
- Low cost
- Implantable
- Provides 3D information
- High signal-to-noise ratio

The proposed IF^{2}D combines the size and ability of implantation of scintillating fibers with the materials used in TLDs to provide integral dose information of the radiation site. This device utilizes f-centers in order to correlate the radiation dose receive and color change in various salts. Since the color change in the salts is a passive occurrence, the dosimeter's continuous operation and dose acquisition is not dependent on data acquisition nor signal processing hardware. Relatively inexpensive hardware is required to study the color changes in salts due to f-centers created from ionizing radiation, such as handheld color spectrometers. Furthermore, a 3D configuration including tiny installations of dosimeters can be made by coupling salt crystals within a fiber optic bundle. The feedback control comes from the ability to differentiate integral dose information when the dosimeter

encounters a known white light source **[9]**. The following figure describes the proposed dosimeter and its individual components.

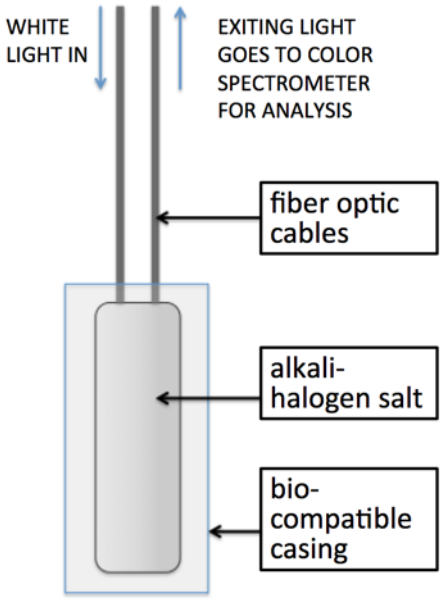

Figure 4 Graphical representation of the proposed fault-tolerant dosimeter and its individual parts. Enclosed the biocompatible casing are color changing alkali-halide salts. A white light with a known spectrum is sent through a fiber optic cable to determine the color of the material. This returns through the second fiber optic cable and reaches the color spectrometer for analysis *[9]*.

The dosimeter will consist of fiber optic cables, a biocompatible casing and alkali halide salts. The biocompatible case contains the salts that will be structurally damaged by the radiation. The fiber optic cables will be used to analyze the color changing alkali halide salts. On one end, white light with a known spectrum enters the device, and on the other end a second fiber optic cable sends light to a color spectrometer for analysis.

We can characterize the color shift of a salt by comparing the exiting light to the original spectrum of a non-irradiated baseline. Then, color absorption can be correlated to radiation damage experienced by the salt and that serves to calculate how much dose the salt has received. The proposed dosimeter can collect this information continuously during the radiation process, and this allows continuous feedback on the dose received.

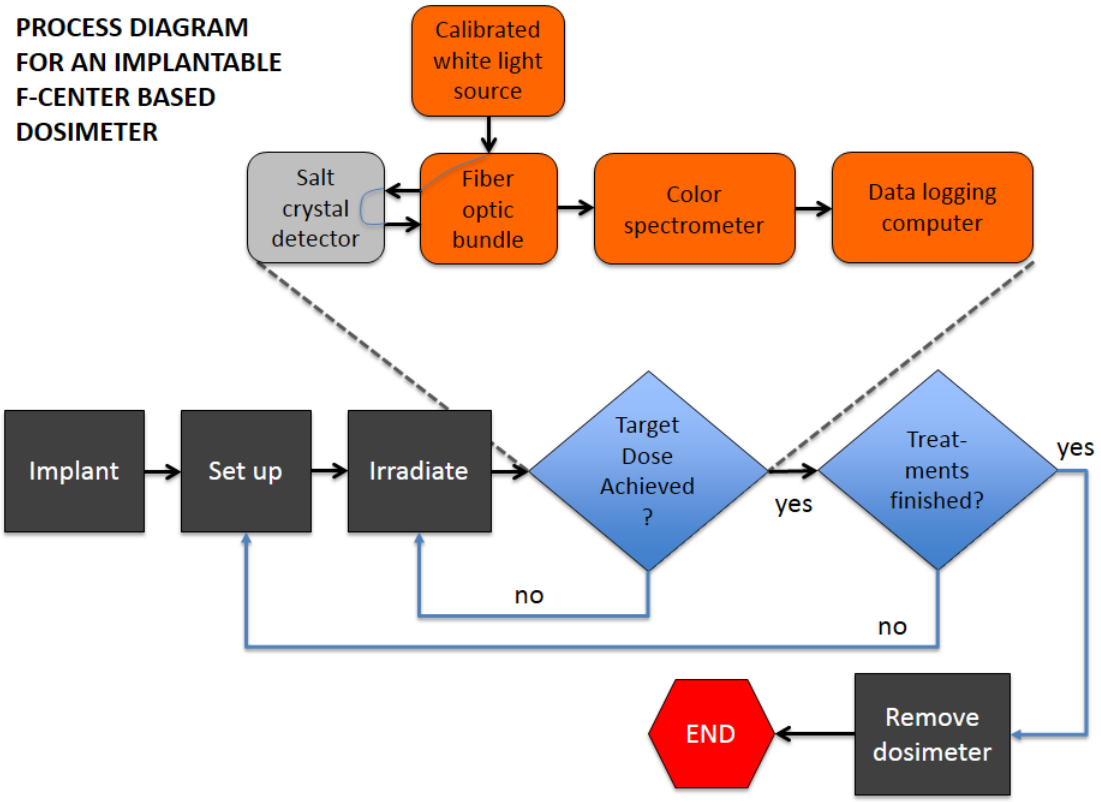

Figure 5 The process diagram for the proposed IF^{2}D which combines two desirable characteristics of the previously mentioned scintillating dosimeter and TLDs: target-measured dose and passively integrating nature of a TLD. Furthermore, it is less invasive and does not need to be removed in between radiation therapy treatments in order to obtain dose information *[9]*.

The figure above is the process diagram for the proposed IF^{2}D. The process begins with implantation of the dosimeter in the patient which may remain in the patient for the duration of the radiation therapy treatment and makes this device less invasive. The IF^{2}D is independent of electronics and hardware for data acquisition. This is due to the f-center behavior of irradiated salts that provide passive information of the radiation dose. As a result, failure or malfunction of any data acquisition component can be replaced individually without losing or compromising data [9].

2.4.1 Comparison to an implantable scintillator dosimeter

One previously developed dosimeter is the implantable scintillator dosimeter. The following process diagram compares the usage procedure between the implantable scintillator and the proposed IF^{2}D. One advantage of the implantable scintillator dosimeter is that it is in-vivo, local dosimetry which means it isn't necessary to estimate the tumor's dose using external dosimetry measurements.

The following figure illustrates the process for an implantable scintillator dosimeter. The first step in the process is implantation; the dosimeter can be implanted in any configuration

in the targeted site and surrounding healthy tissue. Following is the usual radiation therapy setup (which may include CT scans, patient positioning, calculations on intensity and beam time required). During the irradiation procedure, the dosimeter allows for feedback (represented by the blue diamond on the figure) in order to achieve the prescribed dose and end the procedure (represented by the red hexagon) [9].

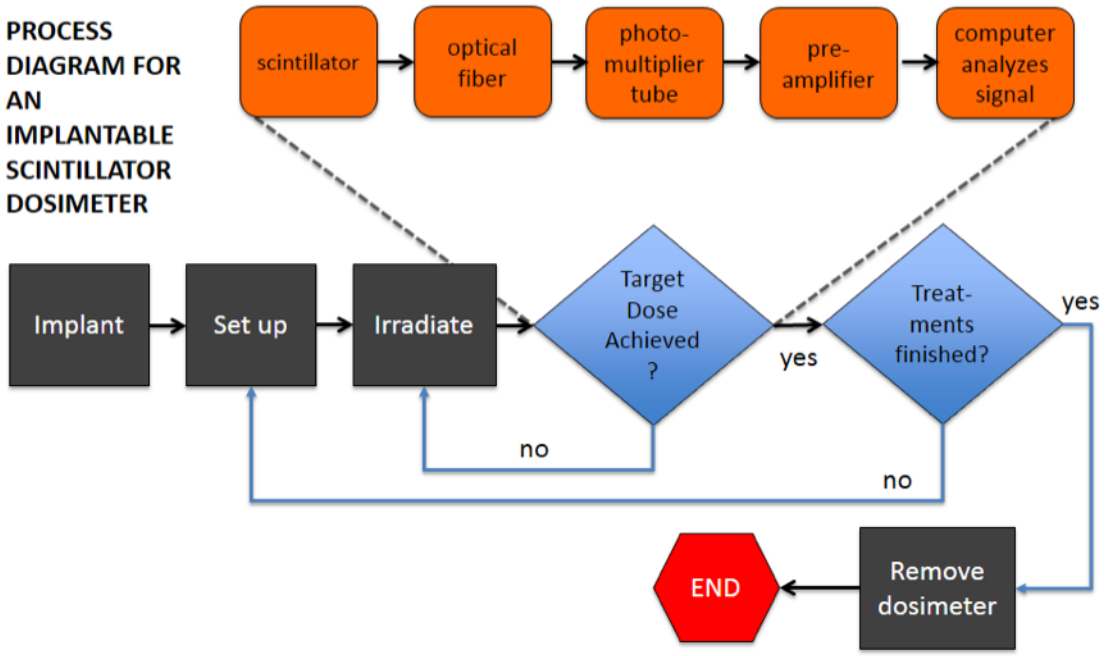

Figure 6 The process diagram for an implantable scintillator dosimeter consists of implantation, set up, irradiation, feedback, and removal. The implantable scintillator dosimeter is dependent on the orange figures for active feedback i.e. if any component fails during the treatment, information is compromised or lost *[9]*.

Although feedback allows corrections in errors made during the initial setup or irradiation steps, it is important to note the steps that must occur successfully to provide effective feedback. The feedback is composed of the scintillator, optical fiber, photomultiplier tube (PMT), PMT pre-amplifier, and software-hardware of the computer. All of these components must work properly throughout the duration of the radiation therapy, or else data will be compromised during the procedure. Data can be lost or compromised because the scintillator is not a naturally integral detector, and any integrated dose information is dependent on the individual components' functions. The IF^2D resolves these issues and works in a passively integral manner: the color change in the salts is a dependent function of irradiation received by the device only. Obtaining data using the IF^2D is not an active component because it conducts periodic interrogation [9].

2.4.2 Comparison to an implantable thermoluminescent dosimeter

Thermoluminescent dosimeters are extensively used for dosimetry externally. The following figure and explanation are related to TLDs used for dosimetry internally. Unlike the implantable scintillator dosimeter, TLDs are natural integral detectors and faulty components won't compromise or lose irradiation information. However, TLDs must be removed from the patient in order to read information and so TLDs do not provide real-time feedback. As a result, the setup and irradiation procedure are susceptible to becoming weak points, since errors in the dose received by the patient are possible and won't be seen until after the procedure. Furthermore, this procedure is more invasive considering the patient goes through multiple medical procedures in order to remove and implant the dosimeter [9].

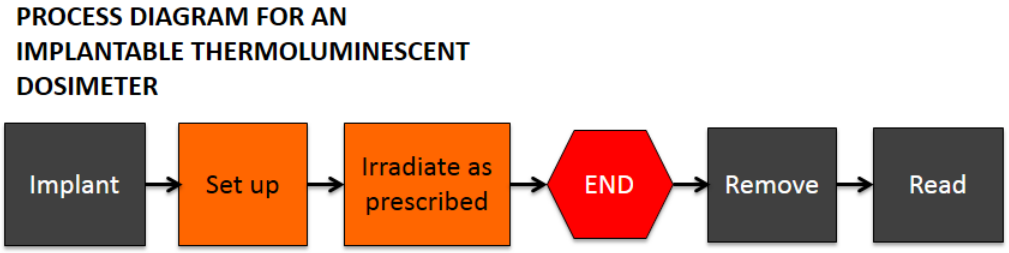

Figure 7 The process diagram for an implantable TLD involves less dependence on individual components to output a dose measurement. However, TLDs require removal in order to read information about irradiated dose and this precludes any online dose measurements *[9]*.

2.4 Salt Selection

Figure 8 Alkali-halide salts chosen for irradiation include NaCl, NaI, NaF, NaBr, and CsF for their distinct f-center behavior and potential applications to IF2D.

Alkali-halide salts present desirable f-center behavior. Salt selection was based on accessibility and individual characteristics. The four Na alkali-halides chosen were: NaCl, NaI, NaF, and NaBr. The fifth salt selected was CsF. Each salt has common uses: NaF is used in toothpaste to prevent dental caries [17]. Temperature conditions were also considered, and x-ray irradiation in particular shows that f-centers are present in room temperature [5].

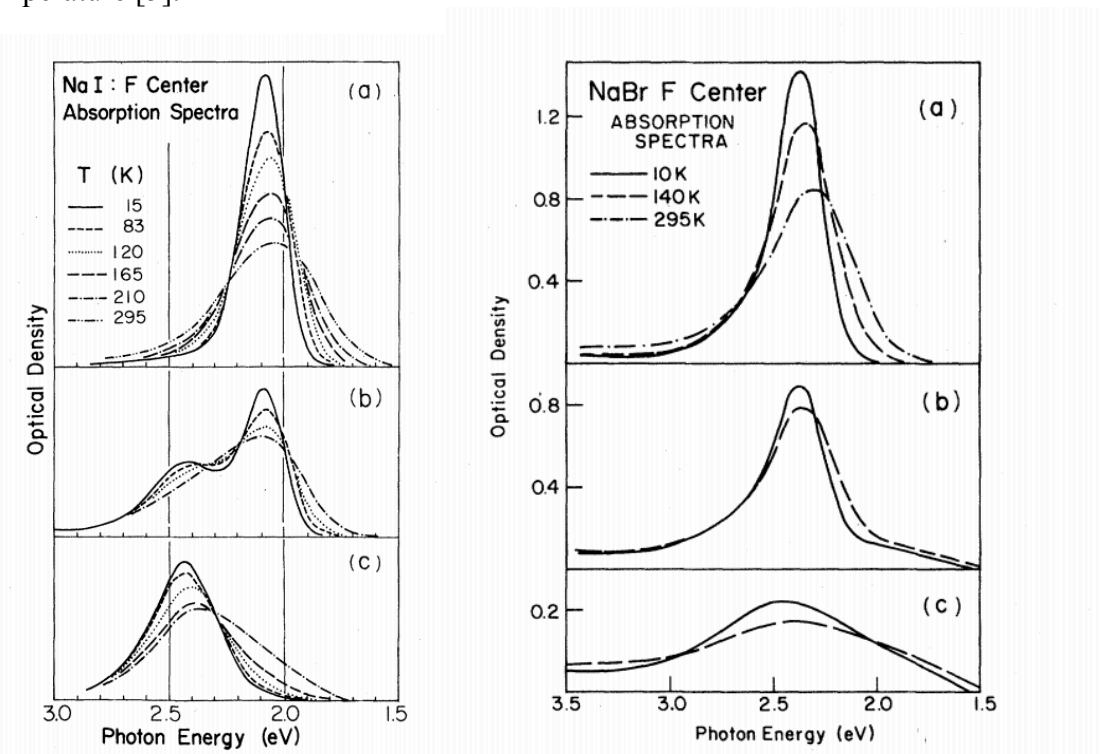

Figure 9 Absorption spectra of colored NaI and NaBr crystals at different temperatures: (a) Pure spectra (b) F-band bleaching at 130 K (absorption scale expanded by a factor of 2 (c) Decomposition of spectra. The experimental data is important for salt selection in the proof of concept for the IF^2D because it concludes a temperature dependence and a clear peak at photon energies of ~2.0 eV *[18]*.

Table 1 Parts list of salts purchased and used for this experiment from STREM Chemicals, INC. at 99.9% Anhydrous.

SALT	CAS NUMBER
NaCl	7647-14-5
NaI	7681-82-5
NaBr	7647-15-6
NaF	7681-49-4
CsF	13400-13-0

Baldacchini used crystals grown in the Utah Crystal Growth Laboratory to analyze f-center behavior in NaBr and NaI. The following figure shows f-center absorption spectra measured in a range of photon energy. The optical density varies and depends on the process taken in a, b, and c. The experimental data is important for salt selection in the proof of concept for the IF^2D because it concludes a temperature dependence and a clear peak at photon energies of ~2.0 eV for NaI and ~2.5 eV for NaBr [18].

3 Methodology

3.1 Salt Preparation

In general, alkali-halide salts present consistent f-center behavior. To take advantage of this characteristic, five salts were chosen based on their f-center behavior and biocompatibility including NaCl, NaI, NaF, NaBr, and CsF. The salts were kept in a desiccator in order to control exposure to the atmosphere and control moisture effects. In order to obtain more accurate results, salts with low opacity i.e. high transparency, are required. The following outlines a procedure that requires revision in order to obtain the desired transparency.

The optimized procedure that has obtained varying results includes 15 g of each chosen salt. A fine consistency is desired which allows for lower opacity, so starting with NaCl, 30 g were measured and grounded using a mortar and pestle (Figure 11).

Figure 10 The CARVER Pellet Press has a 20,000 lb pressure limitation. In this case, a 13 mm pellet die was used that has a pressure limitation of 18,000 lb. This setup includes a vacuum pump to remove any atmospheric effects on the salt being pressed.

Once the salt displayed a consistency similar to confectionary sugar i.e. fine powder, 15 g of NaCl were measured and placed in the 13 mm pellet die. To prepare the salt crystals, the CARVER pellet press (Figure 10) was used with a vacuum pump. The 13 mm pellet die is within the pressure limitation range as the CARVER press used i.e. 18,000 pounds. At maximum pressure, the 15 g of salt were pressed for 15 minutes.

Figure 11 Mortar and pestle used to grind the salts into a fine powder similar to confectionary sugar.

Following the 15 minutes, the salts were removed from the die, were placed in beakers and were returned to the desiccator to avoid atmospheric effects.

An important note is to wash the mortar and pestle after each use. Mixing salts will result in contaminated samples and inaccurate wavelength measurements. Each salt has different and specific reactions to the atmosphere that can change the spectrum observed after irradiation.

3.2 Salt Irradiation

In order to provide a proof of concept of the IF^{2}D, the set of five salts will be irradiated with protons produced from CLASS, a tandem electrostatic accelerator. Typical energies for proton therapy range between 70-250 MeV since protons lose kinetic energy per unit distance. In order to get a full understanding of the salts' f-center behavior energy ranges up to CLASS's 3.4 MeV limit will be recorded using a ThorLabs USB spectrometer in data acquisition.

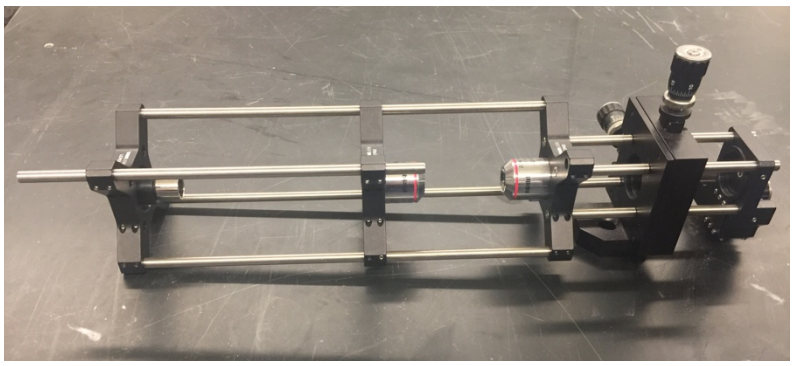

Figure 12 ThorLabs Spectrometer intended for wavelength measurements before and after irradiation. In conjunction with the ThorLabs CCD 100 Spectrometer program, it can be used to compare the light intensity of the salts to obtain a percent absorption.

Before irradiation, using the ThorLabs CCD 100 Spectrometer program, a baseline measurement must be taken of the pressed salt. This baseline will serve as the comparison between the original salt and post-irradiation salt. A comparison of the two will enable percent absorption calculations that can be correlated to radiation dose.

3.3 SRIM Program

In order to record the absorption at different wavelengths of the irradiated salts, the SRIM program can be used in conjunction with the ThorLabs USB spectrometer. The SRIM program calculates ranges and damage rates due to charged particles using a monte carlo approach. In this case, SRIM will calculate the range and damage rates due to the accelerated protons at the different energies operated with CLASS. These calculations will provide a proof of concept of the IF^2D after comparing to the results of the ThorLabs CCD 100 Spectrometer program.

4 Data & Results

4.1 Theoretical Data

An extensive number of sources exist for alkali halide irradiation using x-ray therapy. However, sources are limited in f-center behavior for proton irradiated alkali halides. The following conditions are considered from x-ray irradiated alkali halide behaviors and translated as initial conditions for experimental acquisition.

While doses in proton therapy can reach up to 100 Gy, depending on the location of the tumor, radiation doses are delivered in multiple treatments. As a result, typical treatments can range between 1 Gy - 4 Gy [19]. Therefore, the CLASS tandem accelerator should produce protons in the range up to 3.4 MeV (accelerator's maximum) to measure each salt's wavelengths. Furthermore, proton therapy requires a dose delivery of 2 Gy/min [20], which adds another constraint to the accelerator.

The following theoretical calculations in Table 1 are for KCl and expand on work done by Pooley who found that there is a linear dependence of range on energy that implies a uniform ionization density throughout the irradiated region [21].

Table 2 The expected range at the targeted proton therapy energies of 70-250 MeV. These are theoretical estimates expanding on Pooley's: 7µm range at 400 KeV and 1.5µm range at 100 KeV. Beam currents were at 1 µA and temperature at 4K, KCl crystal had a dimension of 10x10x1 mm with impurities less than 10 ppm.

RANGE	ENERGY	RANGE
1050 µm 0.105 cm	70 MeV	lower
1225 µm 0.1225 cm	70 MeV	higher
3750 µm 0.375 cm	250 MeV	lower
4375 µm 0.4375 cm	250 MeV	higher

4.2 Experimental Data

Due to insufficient transparency in the salts, salt irradiation was postponed for this initial experiment phase. The following results tabulate the different approaches taken in salt preparation and their outcomes.

4.2.1 Salt Preparation

From the optimized salt preparation, the following characteristics were recorded:

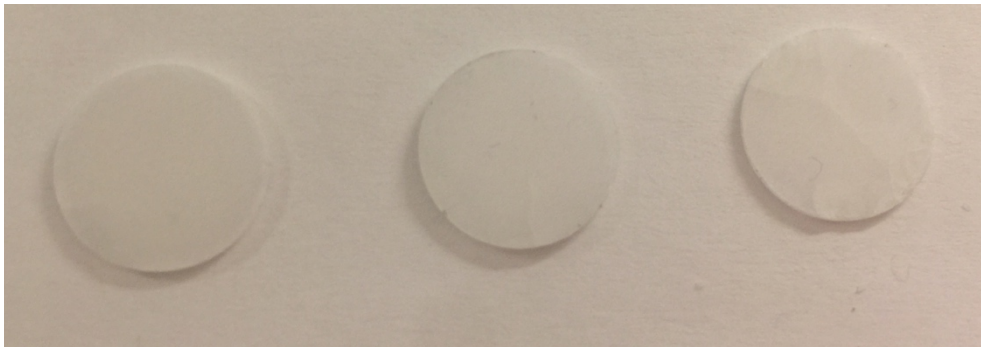

Figure 13 Pellet pressed NaCl at different mass for 15 minutes. From left to right: (a) 20 g Trial 2 (b) 24 g (c) 20g Trial 1

Table 3 Qualitative results of chosen salts with different masses and pellet press time. The characteristics considered are opacity and cracking. The salts that were opaque and cracked will provide more experimental error because they will not be uniform upon irradiation. In this case, a check mark is given to salts that are completely opaque. None of the salts resulted in uniform transparency. The salts in bold indicate the best results with minimized opaque sections.

SALT	MASS (g)	TIME (min)	OPAQUE	CRACKS
NaBr	47 g	15:00	✓	
NaBr	**24 g**	**15:00**		
NaBr	20 g	20:00		✓
NaBr	24 g	20:00		✓
NaBr	15 g	20:00	✓	
NaBr	15 g	15:00	✓	
NaCl	24 g	15:00	✓	
NaCl	20 g	15:00	✓	✓
NaCl	20 g	15:00	✓	
NaCl	**15 g**	**15:00**		
NaI	15 g	15:00	✓	
NaF	15 g	15:00	✓	✓
CsF	15 g	15:00	✓	
KBr	**28 g**	**15:00**		

4.3 Analysis

The salt preparation followed procedures suggested by pellet press experts and common pellet press practice. However, high opacity and some cracking was prevalent in various salts. Initial research indicated that the choice of alkali halides: NaCl, NaBr, NaI, NaF, and CsF, were favorable due to their f-center behaviors and availability. However, NaI, NaF, and CsF require more controlled laboratory conditions for pellet pressing. After 5 minutes of exposure the salts displayed a change in consistency and were no longer anhydrous. Their retention of water led to the highest opacity of the salts. Under stricter environmental conditions, the salts should be pressed until the required transparency is achieved and then placed in the desiccator to avoid increase in opacity.

5 Conclusions

Proton therapy has qualities that reduce the probability of obtaining secondary cancers due to radiation treatments. Unlike photon therapy, proton therapy is characterized by its Bragg peaks that allow for a larger deposit of energy at a concentrated depth in the target tumor. However, the probability of secondary cancers can be reduced further using the IF^2D. Current dosimeters lack a combination of important components implemented to the IF^2D like: real-time dose, fault tolerance, and implantability.

In order to provide a proof of concept for the proposed dosimeter, alkali halide salts with high transparency are required to maximize the percent absorption vs. dose. Future work includes finding the best pressure to achieve desired transparency. Based on initial pellet pressing, each salt will require a different mass and pressure ratio. The salts that have shown the best transparency using the CARVER pellet press are NaBr, NaCl, and KBr. Further trials with this pellet press are recommended for these three salts. However, the rest of the salts require a press with a higher-pressure limit and a pellet die with a high-pressure limit. Recommended mass for initial pressing of these salts is 15 g.

Future work includes irradiating alkali halide salts with the lowest opacity achievable using the CLASS tandem electrostatic accelerator. Based on initial investigation and calculation, the accelerator must irradiate salts to obtain a dose of 1 Gy - 4 Gy at a dose rate of $\frac{2Gy}{min}$. This correlates with proton therapy standards and will provide a direct proportionality between the dosimeter measurements and expected results when implemented in radiation therapy.

References

[1] H. Paganetti, Proton Beam Therapy, Boston, Massachussetts: IOP Publishing, 2017.

[2] S. Yip, Nuclear Radiation Interactions, Massachussetts: World Scientific Publishing Co., 2015.

[3] "Zigya," [Online]. Available: https://bit.ly/2Ig8LkB. [Accessed 5 May 2018].

[4] J. H. Schulman and W. D. Compton, "Color centers in solids," *Oxford: Pergamon Press,* p. 368, 1962.

[5] F. Seitz, "Color centers in alkali halide crystals," *Reviews of Modern Physics,* vol. 18, 1946.

[6] I. L. Mador and et al., "Production and bleaching of color centers in x-ray alkali halide crystals," *Phys. Rev.,* vol. 96, no. 3, 1954.

[7] J. Arends and et al., "F-Center Formation in Mixed Crystals," *Phys. Stat. Sol.,* vol. 10, pp. 105-112, 1965.

[8] C. De Wagter, "The ideal dosimeter for intensity modulated radiation therapy (IMRT): What is required?," *J. Phys.: Conf. Series ,* vol. 3, no. 1, 2004.

[9] M. P. Short, D. R. Gupta , S. Ferry and C. Dennett, *Fault-Tolerant, Passively Integrating In-vivo dosimeters for feedback-enabled radiation therapy (IF2D, or Integrating Feedback F-center Dosimeter),* Cambridge, MA, 2016.

[10] C.-H. Min et al., "Prompt gamma measurements for locating the dose falloff regin in the proton therapy," *Appl. Phys. Lett.,* vol. 89, no. 18, 2006.

[11] F. Stichelbaut and Y. Jongen, "Verification of the proton beam position in the patient by the detection of prompt gamma-rays emission," in *39th PTCOG meeting*, San Francisco, 2003.

[12] P. Gueth et al., "Machine learning-based patient specific prompt-gamma dose monitoring in proton therapy," *Phys. in Med. Bio.,* vol. 58, no. 13, 2013.

[13] A. C. Knopf et al., "Accuracy of proton beam range verification using post-treatment positron emission tomography/computed tomography as a function of treatment site," *Intl. J. Rad. Oncology Bio. Phys.,* vol. 79, no. 1, 2011.

[14] R. Ramaseshan et al., "Performance characteristics of a microMOSFET as an in vivo dosimeter in radiation therapy," *Phys. Med. Bio.,* vol. 49, no. 17, 2004.

[15] C. W. Scarantino et al., "An implantable radiation dosimeter for use in external beam radiation therapy," *Med. Phys.,* vol. 31, 2004.

[16] G. P. Beyer et al., "Technical evaluation of radiation dose delivered in prostate cancer patients as measured by an implantable MOSFET dosimeter," *Intl. J. Rad. Oncology,* vol. 69, no. 3, 2007.

[17] S. Kim, P. A. Thiessen, E. E. Bolton, J. Chen, G. Fu, A. Gindulyte, L. Han, J. He, S. He, B. A. Shoemaker, J. Wang, B. Yu, J. Zhang and S. H. Bryant , "PubChem," 4 January 2016. [Online]. Available: https://pubchem.ncbi.nlm.nih.gov/compound/sodium_fluoride#section=Top.

[18] G. Baldacchini, D. S. Pan and F. Lüty, "Radiative and nonradiative processes of F and F' centers in NaBr and NaI," *Physical Review B,* vol. 24, no. 4, 15 August 1988.

[19] H. Liu and J. Y. Chang, "Proton Therapy In Clinical Practice," *Chinese Journal of Cancer,* vol. 30, no. 5, pp. 315-326, 2011.

[20] H. Paganetti and T. Bortfeld, "AAPM," [Online]. Available: https://www.aapm.org/meetings/05am/pdf/18-4016-65735-22.pdf. [Accessed 5 May 2018].

[21] D. Pooley, "The saturation of F-centre production in alkali halides under proton irradiation," *Brit. J. Appl. Phys.,* vol. 17, pp. 855-861, 1996.

[22] W. P. Levin, H. Kooy, J. S. Loeffler and T. F. DeLaney, "Proton beam therapy," *British Journal of Cancer,* vol. 93, pp. 849-854, 17 October 2005.

[23] D. Pooley and W. A. Runciman, "Recombination luminescence in alkali halides," *Journal of Physics C: Solid State Physics,* vol. 3, no. 8, 1970.

[24] H. Von Seggern, A. Meijerink, T. Voigt and A. Winnacker, "Photosimulation mechanism x-ray irradiated RbBr:Tl," *Journal of Applied Physics,* vol. 66, no. 9, pp. 4418-4424.

[25] N. Itoh and K. Tanimura, "Formation of interstitial-vacancy pairs by electronic excitation in pure ionic-crystals," *Journal of Physics C: Solid State Physics,* vol. 51, pp. 717-735, 1990.